Journal of Materials Chemistry A

PAPER

View Article Online
View Journal | View Issue

Cite this: J. Mater. Chem. A, 2015, 3, 6004

New insights into the electrochemical performance of Li_2MnSiO_4: effect of cationic substitutions†

A. Saracibar,[abc] Z. Wang,[d] K. J. Carroll,[de] Y. S. Meng[d] and M. E. Arroyo-de Dompablo*[a]

Received 1st July 2014
Accepted 1st February 2015

DOI: 10.1039/c4ta03367a

www.rsc.org/MaterialsA

The performance of the Li_2MnSiO_4 cathode material is hindered by voltage decay and capacity fading caused by structural instability. To rationalize the origin of such structural instability, we have investigated a total of 142 $Li_{2y}MnSiO_4$ configurations at $y = 0.125$, 0.25, 0.333, 0.375, 0.417, 0.5, 0.625, 0.666, 0.75 and 0.875 by density functional theory methods. It is found that the most stable $Li_{2y}MnSiO_4$ configurations with $y \leq 0.5$ consist of Mn^{4+} and Mn^{3+} in octahedral or five-fold coordination. This induces a crystal deformation, loss of the orthogonal symmetry, and a notorious volume decrease (7% for $LiMnSiO_4$ and 14% for $Li_{0.5}MnSiO_4$). The effect of Mn substitution on the crystal structure of the delithiated silicates $Li_{0.5}Mn_{0.75}M_{0.25}SiO_4$ is computationally investigated for M = Mg, Fe, Co and Ni. The most stable configurations for Mg, Fe and Co substitutes possess Mn^{4+} in octahedral coordination, sharing edges with the adjacent Si and Mn polyhedra. DFT results suggest that among the studied substituents, only Ni could help to maintain the structural integrity of the delithiated samples. Experimentally, $Li_2Mn_{1-x}Ni_xSiO_4$ samples with $x = 0$, 0.1 and 0.2 were synthesized and electrochemically tested.

Introduction

Lithium-ion batteries are essential in portable electronics and are becoming a competitive technology for larger-scale application in transportation and grid stabilization of renewable sources (*i.e.* wind and solar). However, to support the increasing demand for energy and power, urgent improvements are needed; one of the current strategies is to increase the specific capacity. In this sense, lithium transition metal (Li_2MSiO_4, M = Fe, Mn, Co, Ni) silicate materials have been presented as promising cathode materials for lithium ion batteries.[1–4] The key advantage of these silicates is their theoretical capability to reversibly de-intercalate two lithium equivalents from the structure, giving a very high theoretical capacity of about 333 mA h g^{-1}. The most promising candidates are the Li_2FeSiO_4 and Li_2MnSiO_4. With Fe redox potentials at 3.1 V (Fe^{2+}/Fe^{3+}) and 4.7 V (Fe^{3+}/Fe^{4+}) and both Mn redox potentials (Mn^{2+}/Mn^{3+} and Mn^{3+}/Mn^{4+}) mixed at 4.0 V, these materials have electrochemical processes within the stability of organic electrolytes, this is, up to *ca.* 4.8 V against a Li^+/Li electrode.[5]

The crystal structure of Li_2MSiO_4 consists of a distorted hexagonal packing of oxygen ions with half of the tetrahedral sites occupied by Li, M and Si.[6] A large number of Li_2MSiO_4 polymorphs are possible by assuming a different pattern of occupancy of the tetrahedral voids in the distorted hexagonally packed anion framework. Fig. 1a shows the crystal structure of the $Pmn2_1$ polymorph which has been determined as the most stable polymorph for M = Fe and Mn.[7–9] The crystal cell consists of only corner-sharing tetrahedra, all pointing toward the same orientation along the *c* axis. It is a 2-D structure built up from infinite corrugated layers of composition $[SiMO_4]_\infty$ lying on the *ac*-plane and linked along the *b*-axis by LiO_4 tetrahedra.

For the two electron process, Li_2MnSiO_4 provides more advantages than Li_2FeSiO_4. Since in Li_2MnSiO_4 the voltage jump between the first and second lithium extraction does not proceed through the large jump that Li_2FeSiO_4 encounters,[4,5] Li_2MnSiO_4 offers the possibility of the second lithium extraction at a lower cell voltage. A recent review discusses the preparation techniques, structural issues, conductivity enhancement and complex morphologies of reported Li_2MnSiO_4 electrode materials.[10] Unfortunately many experimental efforts have failed to achieve a good electrochemical performance even in the one electron process, due to the structural instability of Li_2MnSiO_4 upon delithiation.[5,10–15] Calculations at the Density Functional Theory level (DFT) support the tendency of the Li_2MnSiO_4 structure to collapse upon delithiation of more than one Li ion.[5,13] Attempts have also been made to stabilize the crystal structure of delithiated Li_2MnSiO_4 by partial Fe substitution for Mn, as suggested by DFT

[a]Dpto. de Química Inorgánica, Facultad de Ciencias Químicas, Universidad Complutense de Madrid, 28040-Madrid, Spain. E-mail: e.arroyo@quim.ucm.es
[b]Dpto de Química Física, Facultad de Farmacia, Ps de la Universidad, 7 01006 Vitoria-Gasteiz, Spain
[c]CIC-Energigune, Parque Tecnológico de Álava, Albert Einstein, 48. Edificio CIC, 01510 Miñano, Álava, Spain
[d]Department of NanoEngineering, University of California San Diego, La Jolla, CA 92037, USA
[e]Department of Chemical Engineering, Massachusetts Institute of Technology, Cambridge, MA 01239, USA

† Electronic supplementary information (ESI) available. See DOI: 10.1039/c4ta03367a

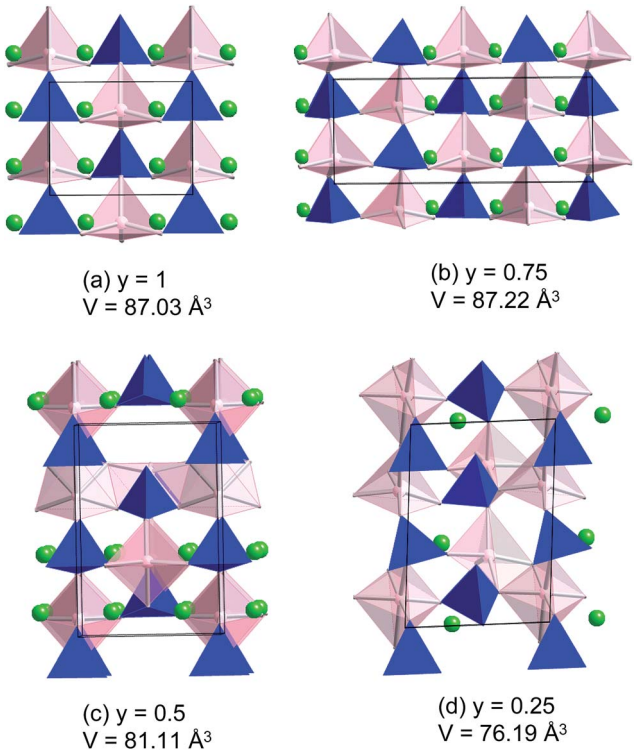

Fig. 1 Crystal structure of $Pmn2_1$-$Li_{2y}MnSiO_4$ (a) at $y = 1$, (b) $y = 0.75$, (c) $y = 0.5$ and (d) $y = 0.25$ along the b axis. The cell volume (in $Å^3$) is given per formula unit. Color code: Li green, Mn pink and Si blue.

calculations.[13] Several studies were conducted in that direction; to date, the $Li_2Mn_{1-x}Fe_xSiO_4$ electrode materials have shown a poor reversibility and cycling stability.[10] To the best of our knowledge, the electrochemistry of other substituted $Li_2Mn_{1-x}M_xSiO_4$ electrode materials has not been reported.

Currently, a rational explanation of the structural instability of the delithiated $Li_{2y}MnSiO_4$ phases is still lacking. This understanding is important to route the experimental efforts in the possible modifications that could lead to improved electrochemical characteristics. In the present work, we investigate and rationalize the origin of the crystal distortion in Li_2MnSiO_4 silicates upon delithiation. DFT results suggest that the structural instability is related to the trend of Mn^{3+}/Mn^{4+} ions to adopt an octahedral coordination. DFT is a powerful tool to anticipate the effect of cationic substitutions on the electrochemical properties of Li_2MnSiO_4. Aiming to improve the electrode characteristics of Li_2MnSiO_4 we have explored the role of Mg, Fe, Co and Ni as possible substitutes for Mn ($Li_{2y}Mn_{0.75}M_{0.25}SiO_4$). We will show that Mn substitution by Ni might help to prevent the structural collapse. A novel experimental investigation of the $Li_2Mn_{1-x}Ni_xSiO_4$ electrode materials is finally presented.

Methodology

Computational

The total energies of $Li_{2y}MSiO_4$ were calculated using the *ab initio* methods implemented in the Vienna *Ab initio* Simulation Package (VASP).[16–18] The Projector Augmented Wave (PAW) potential set[19] was used with the exchange and correlation energies approximated in the generalized gradient approximation with the Hubbard parameter correction (GGA + U) following the rotationally invariant form.[16,20] An effective U value of 4 eV ($J = 1$ eV) was used for the d states of TM ions. The energy cut off for the plane wave basis set was kept fixed at a constant value of 600 eV throughout the calculations. The integration in the Brillouin zone is done on an appropriate set of k-points determined by the Monkhorst–Pack scheme. A convergence of the total energy close to 5 meV per formula unit is achieved with such parameters. The structures were fully relaxed (cell parameters, volume cells and atomic positions).

The initial atomic positions for Li_2MnSiO_4 were taken from the proposed orthorhombic structure for Li_2MnSiO_4 (space group $Pmn2_1$) which is the most stable one. For the intermediate phases, $Li_{2y}MnSiO_4$ lithium-vacancy arrangements have been created using the CASM (Cluster-Assisted Statistical Mechanics) software package.[21,22] We have computed a total of 142 configurations in the $Pmn2_1$ host, using supercells of up to 6 formula units ($Li_{12}Mn_6Si_6O_{24}$). The investigated $Li_{2y}MnSiO_4$ configurations have y values of 0.125, 0.25, 0.333, 0.375, 0.417, 0.5, 0.625, 0.75 and 0.875. For the half delithiated phase ($y = 0.5$), we have tested up to 35 different lithium-vacancy arrangements.

Substituted $Li_{2y}Mn_{0.75}M_{0.25}SiO_4$ (M = Mg, Fe, Co, and Ni) silicates have been investigated for $y = 0.75$ and $y = 0.25$ with a unit cell containing 4 formula units. The lithium-vacancy ordering corresponds to the detected ground state for the pure Mn silicate. The calculations have been initialized incorporating the lithium vacancies in the pristine Li_2MnSiO_4 crystal structure (orthogonal $Pmn2_1$ symmetry). Any possible ordering of Mn and M ions within this cell was also computed. Cell volume and shape together with atomic positions have been fully relaxed.

Experimental

Among the various synthesis routes utilized to prepare Li_2MnSiO_4, the solvothermal synthesis has produced the materials with the best electrochemical characteristics. In this work, we have prepared $Li_2Mn_{1-x}Ni_xSiO_4$ ($x = 0$, 0.1, 0.2) compounds utilizing the solvothermal method used by Aravindan *et al.*[23] $NiCl_2{\cdot}6H_2O$ and $MnCl_2{\cdot}4H_2O$ (Sigma Aldrich, 99.99%) were used in proportions to produce $Li_2Mn_{1-x}Ni_xSiO_4$ ($x = 0$, 0.1, 0.2). First, 0.386 g (0.0092 mol) of $LiOH{\cdot}H_2O$ was added to 5 mL of deionized water. Then, 0.138 g (0.0023 mol) of SiO_2 was added to the solution and sonicated for one hour. Meanwhile, a total of 0.0023 mol of transition metal chlorides with appropriate ratios were dissolved in 10 mL of ethylene glycol by stirring. The two solutions were then combined and further stirred for one hour before placing in a 23 mL Parr 4749 acid digestion vessel. The vessel was heated at 150 °C for 48 hours and the product was filtered and dried at 60 °C overnight. For carbon coating, the as-synthesized material was mixed with 30 wt% sucrose (Sigma Aldrich > 99.5%) and pelletized. The pellet was then heated at 700 °C in an Ar atmosphere for 10 hours.

Powder X-ray diffraction patterns were taken on a Siemens D-5000 and X'Pert Pro Alpha I laboratory X-ray diffractometer. Electrochemical properties were measured on an Arbin battery cycler in galvanostatic mode. Cathodes were prepared by mixing the active material with 10 wt% Super P carbon (TIMCAL) and 10 wt% poly-vinylidene fluoride (PVDF) (from Arkema) in *N*-methyl pyrrolidone (NMP) solution. The batteries were prepared in an argon glove box using the lithium metal anode and a 1 M $LiPF_6$ in a 1 : 1 ethylene carbonate–dimethyl carbonate (EC : DMC) electrolyte solution (Novolyte). The Celgard model C480 separator (Celgard Inc, USA) was used as the separator.

The charged samples for XPS were recovered by disassembling cycled batteries in an argon-filled glove box and washed with acetonitrile several times. X-ray photoelectron spectroscopy (XPS) data were collected using a Thermo Fisher Scientific K-Alpha XPS using monochromatic Al K-alpha X-rays (1486.6 eV). The instrument was equipped with a six element multichannel detector where the incident beam was 45° off normal to the sample while the X-ray photoelectron detector was normal to the sample. Charge compensation was employed during data collection by using an internal flood gun (2 eV electrons) and a low energy Ar^+ external flood gun. The chamber pressure was kept $<10^{-8}$ Torr during the measurements. High-resolution data were collected at pass energies of 5.85 eV with 0.05 eV step sizes and a minimum of 15 scans. The energy of the spectra was calibrated by the binding energy of the hydrocarbon C1s (C–H) at 284.6 eV, which corresponds mainly to adventitious carbon. The data were analyzed using the software CasaXPS and all peaks were fit using a Shirley-type background function. Powder samples were mounted onto the XPS holder *via* double-sided carbon tape.

Results and discussion

(A) Formation energies and ground states in Li_2MnSiO_4

We have evaluated the stability of $Li_{2y}MnSiO_4$ ($0 < y < 1$) phases according to the reaction:

$$y\mathrm{Li_2MnSiO_4} + (1 - y)\mathrm{MnSiO_4} \rightarrow \mathrm{Li_{2y}MnSiO_4} \quad (1)$$

Fig. 2 shows the formation energies of the computed 142 different lithium vacancy arrangements. The formation energy of $Li_{2x}MnSiO_4$ is defined as:

$$\Delta_f E = E - yE_{\mathrm{Li_2MnSiO_4}} - (1 - y)E_{\mathrm{MnSiO_4}} \quad (2)$$

where E is the total energy of the $Li_{2y}MnSiO_4$ configuration per formula unit, $E_{Li_2MnSiO_4}$ is the totally energy of the lithiated phase and E_{MnSiO_4} is the energy of the delithiated $Pmn2_1$ $MnSiO_4$ host. The convex hull (line connecting the lowest phases in the formation energy *versus* composition curve) is displayed in Fig. 2. While for Li_2FeSiO_4 the convex hull is governed by a unique and pronounced ground state at $y = 0.5$ (see ref. 9), the convex hull of Li_2MnSiO_4 presents ground states at $y = 0.125$, $y = 0.5$ and $y = 0.25$.

The crystal structures of the most stable $Li_{2y}MnSiO_4$ configurations at $y = 0.75$, $y = 0.5$ and $y = 0.25$ are shown in Fig. 1. The

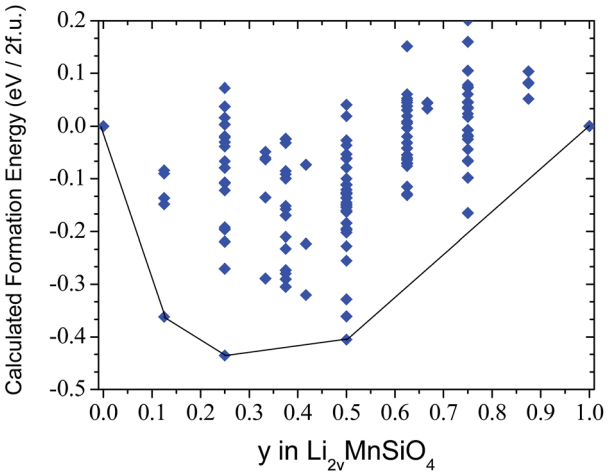

Fig. 2 Formation energies and convex hull of the 142 configurations of $Li_{2y}MnSiO_4$ calculated from first principles.

Mn–O bond distances are listed in the ESI.† The oxidation state around each Mn ion was approximated by integrating the unpaired electron density within a sphere of radius 3.0 Å, but excluding the density coming from the oxygen ions (see Fig. 1 in the ESI†). The most stable configuration at $y = 0.75$ consists of half Mn^{2+} and half Mn^{3+}, all of them retaining the tetrahedral coordination of the pristine material. At this level of delithiation, minor structural distortions are predicted with a cell volume variation of only 0.2%, though with a small deviation from the orthogonal symmetry ($\gamma = 93°$).

From the 35 explored arrangements at $y = 0.5$, the most stable structure (displayed in Fig. 1c) consists of a supercell containing four Li_2MnSiO_4 formula units, with two of the four Mn^{+3} ions presenting a five-fold coordination, and the other two a six-fold coordination with four short distances and two long ones (2.9 Å). When analyzing the observed distortion in depth, it turns out that the coordination change in manganese is accompanied by significant changes in O–Mn–O angles. Distortions of $Li_{2y}MnSiO_4$ materials dominated by changes in O–Mn–O angles have been reported by other authors.[5,25] The predicted cell volume contraction respective to Li_2MnSiO_4 is 6.8% and there is a deviation from the orthogonal symmetry ($\gamma = 87°$). Note that this volume variation is greater than that predicted previously 0.37% in ref. 5 and 2.0% in ref. 13 where only the three possible configurations in the unit cell (two formula units) were considered. In the present work, a deeper analysis of $LiMnSiO_4$ configurations allows the prediction of crystal modifications consistent with the poor cycling retention of Li_2MnSiO_4 even for the one electron process.

In the ground state at $y = 0.25$ ($Li_{0.5}Mn_{0.5}{}^{3+}Mn_{0.5}{}^{4+}SiO_4$) the Mn^{3+} and Mn^{4+} ions are in quite distorted five-fold or six-fold coordination (Fig. 1d). The cell volume diminished 13.7% respective to the pristine material. In addition, the cell distorts losing the orthogonal shape ($\alpha = 85°$ $\beta = 90°$ $\gamma = 75°$) and edge sharing polyhedra are distinguished. Analysis of other low energy $Li_{2y}MnSiO_4$ configurations confirms that at low Li contents ($y \leq 0.5$) the Mn ions do not retain a tetrahedral coordination.

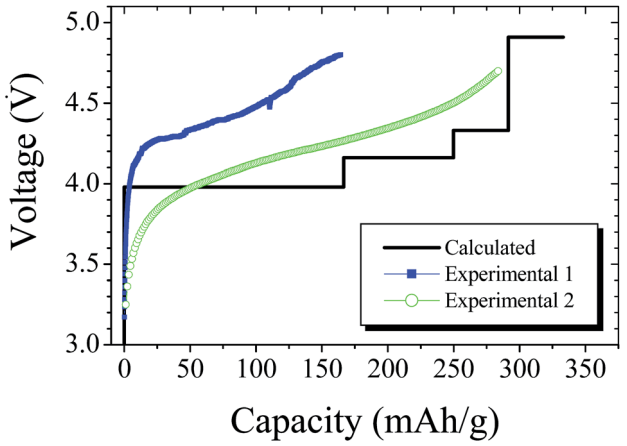

Fig. 3 Calculated charge curve of Li_2MnSiO_4 (in black) compared to the experimental curve taken from Muraliganth *et al.* (experimental 2, in green)[24] and that collected in this work (experimental 1, in blue).

Due to the large crystal distortions in delithiated materials it is not possible to perform a cluster expansion of the calculated formation energies and using it in Monte Carlo methods to simulate the voltage-composition curve[26] of Li_2MnSiO_4 as was done for Li_2FeSiO_4,[9] and layered-$LiMO_3$ (M = Co, Ni) materials.[27] Yet, a scratch of the voltage profile can be extracted from the calculated total energy of the ground states lying on the convex hull. Fig. 3 shows the sketch of the voltage–capacity curve of Li_2MnSiO_4 at 0 K, compared with the experimental profile collected in this work (experimental 1) and with the profile taken from Muraliganth *et al.*[24] (experimental 2). As discussed below our experimental setting results in a lower specific capacity than that obtained in ref. 24. In the calculated profile, for the specific capacity below 300 A h kg^{-1}, the voltage steps between two consecutive single phase regions are small (around 0.15 V). Above 0 K, entropy effects would smooth the voltage-composition profile, resulting in a sloping voltage curve with no detectable ordered phases in agreement with experimental observations. At *ca.* 300 A h kg^{-1}, a greater voltage jump of 0.55 V is predicted, which corresponds to the de-insertion of 1.75 Li ions (formation of $Li_{2y}MnSiO_4$ with $y = 0.125$). The calculated average voltage for this last voltage plateau is 4.9 V. This voltage jump seems consistent with the experimental curve, even though the maximum theoretical capacity (333 A h kg^{-1}) has not been reached in practice.

Comparison of the electrode characteristics of Li_2FeSiO_4 and Li_2MnSiO_4 showed that both materials are stable in the 2D-$Pmn2_1$ polymorph, though various 2D and 3D polymorphs compete in energetic stability, all of them have very similar de-intercalation voltages. For Li_2FeSiO_4, due to the high stabilization of the d^5 configuration, at half delithiation a unique very stable configuration lies in the convex hull. This causes a pronounced voltage step of 2 V in the electrochemical curve at $y = 0.5$. In all the investigated 2D and 3D $Li_{2y}FeSiO_4$ ($0 < y < 1$) configurations the crystal cell maintains the orthorhombic shape and Fe cations appear in tetrahedral coordination. Upon delithiation the system is driven by the need for minimizing electrostatic repulsions, which are ameliorated in the 3D polymorphs. For this reason, Li_2FeSiO_4 suffers from a phase transformation upon delithiation. Unfortunately, delithiation of the 3D structure is accompanied by a large volume variation (around 20%), which precludes the reversible intercalation of the two Li ions.

Table 1 Crystal field stabilization energy (CFSE) for Mn ions in square pyramid (SP), octahedral (Oh) and tetrahedral (Th) environments

Ion	SP (Dq units)	Oh (Dq units)	Th (Dq units)
Mn^{+2}, $Fe^{3+}(d^5)$	0	0	0
Mn^{+3}, $Fe^{4+}(d^4)$	−9.14	−6	−4
$Mn^{+4}(d^3)$	−10	−12	−8

Unlike Li_2FeSiO_4, the fully de-inserted $MnSiO_4$ is more stable in the 2D structure than in a 3D structure.[7] Recent data from Lee *et al.*[28] support this result, though these authors predict an unreasonable voltage-composition curve with the deinsertion voltage of the first lithium from Li_2MnSiO_4 above that of the second lithium ion. In the present work from the analysis of the most stable configurations, we can conclude that lithium de-intercalation from Li_2MnSiO_4 irremediably causes a local distortion of the Mn polyhedra, severe crystal structure deformation, and large volume contraction. None of these features are found in delithiated 2D or 3D-$Li_{2y}FeSiO_4$ ($0 < y < 1$) configurations.

Differences between $Li_{2y}FeSiO_4$ and $Li_{2y}MnSiO_4$ are not surprising; for isostructural compounds, the electronic configuration of the transition metal ion plays a role in the phase stability upon lithium deinsertion.[27] Table 1 lists the crystal field stabilization energies in the 6-fold, 5-fold and 4-fold coordination for Mn ions in different oxidation states. The closed shell Mn^{2+} is equally stable in any coordination. Mn^{+3} is more stable in the square pyramidal coordination, and Mn^{+4} is more stable in the octahedral coordination. Though Mn^{3+} can retain the tetrahedral coordination (see for instance Fig. 1b and c), its tendency to adopt other environments could be assisted by the Li-vacancy ordering. In short, we suggest that the disappearance of the tetrahedral environment of the manganese upon Li removal explains the observed poor reversibility and/or capacity fading of Li_2MnSiO_4 electrode materials.

(B) Crystal structure and energetics of substituted $Li_{0.5}Mn_{0.75}M_{0.25}SiO_4$

The trend of Mn^{3+} and Mn^{4+} to adopt environments other than tetrahedral geometry is inherent to the nature of those ions. Yet we cannot discard that structural changes of $Li_{2y}MnSiO_4$ could be ameliorated by cation substitution. Starting from the unrelaxed ground state of $Li_{1.5}MnSiO_4$ and $Li_{0.5}MnSiO_4$ we have partially substituted 25% of Mn ions for Mg, Fe, Co and Ni. Such cations, together with Zn, are present in tetrahedral Li_3PO_4-type compounds.[6] In a previous investigation[9] we found that for the Li_2MSiO_4 polymorphs, Fe, Mn and Ni stabilize the 2D-$Pmn2_1$ structure, while Co and Mg are more stable in the 3D-$Pbn2_1$ structure. This selection of cations with different electronic configurations and polymorphic stability offers a wide view of possible substituents for Mn ions in Li_2MnSiO_4.

In the $Li_6Mn_3MSi_4O_{16}$ cell, there are two distinct configurations to accommodate the $Li_{1.5}Mn_{0.75}M_{0.25}SiO_4$ stoichiometry. All the optimized configurations contain Mn and M ions in tetrahedral coordination, with similar deviation from orthogonal symmetry to $Li_{1.5}MnSiO_4$ ($\gamma \sim 93°$). The Mg, Co and Ni substituents are in a divalent state (M^{2+}), coexisting with 25% Mn^{2+} and 50% Mn^{3+}. In $Li_{1.5}Mn_{0.75}Fe_{0.25}SiO_4$ the charge distribution is 25% Fe^{3+}, 25% Mn^{3+} and 50% Mn^{2+}. The cell volume follows the trend of the ionic radii of the present divalent cations: $VMn^{2+} > VCo^{2+} > VMg^{2+} > VNi^{2+}$. In short, at this level of delithiation all the substituents retain the structural integrity of the lithiated phase.

In the unit cell of $Li_2Mn_4Si_4O_{16}$ there are four distinct configurations to accommodate the $Li_{0.5}Mn_{0.75}M_{0.25}SiO_4$ stoichiometry. Fig. 4 compares the relative total energy of the four optimized configurations, labelled as 1, 2, 3 and 4. The most stable configuration for each M has been set at the zero energy. In all these configurations, we have analysed the coordination number and the net spin around M ions (Table 2 and Fig. 2 in the ESI†). We found that Mn ions may adopt coordination numbers of 4, 5 and 6, with the latter being restricted to the 4+ oxidation state. Configurations possessing Mn ions in tetrahedral coordination are indicated by a pink circle in Fig. 4. Configurations where octahedral Mn^{4+} is present are denoted by cyan rectangles.

For a given M, the energy difference between configurations can be as large as 0.25 eV per f.u. As seen in Fig. 4, the tetrahedral configuration for all Mn ions destabilizes the structures, while those configurations with Mn^{4+} in octahedral coordination are the most stable. The relative stability certainly depends on the nature of the M ion; the most stable configurations are 1 for Mg, 2 for Ni and 3 for Fe and Co. Fig. 5 shows the optimized most stable structure for each TM, with the atomic distances given in Table 2 in the ESI.† Clear distortions are observed, with none of the substituents retaining the tetrahedral-based framework of the pristine compound. Deviations from the orthogonal symmetry are similar to those observed in the unsubstituted Mn phase ($\alpha = 85°$ $\beta = 90°$ $\gamma = 75°$).

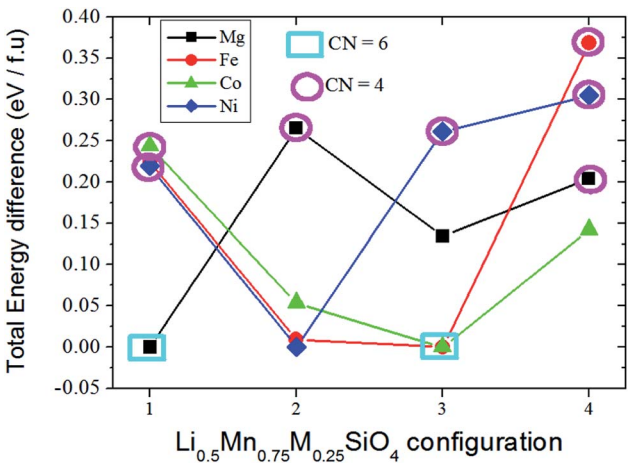

Fig. 4 Calculated total energy difference for the four $Li_{0.5}Mn_{0.75}M_{0.25}SiO_4$ configurations investigated with M = Mg, Fe, Ni and Co. Pink circles/cyan rectangles indicate structures where tetrahedral/octahedral Mn ions are detected.

Table 2 Cell parameters (in Å) of as-prepared $Li_2Mn_{1-x}Ni_xSiO_4$ with $x = 0$, 0.1, 0.2

x	a	b	c
0	6.314	5.389	4.967
0.1	6.311	5.383	4.968
0.2	6.308	5.383	4.964

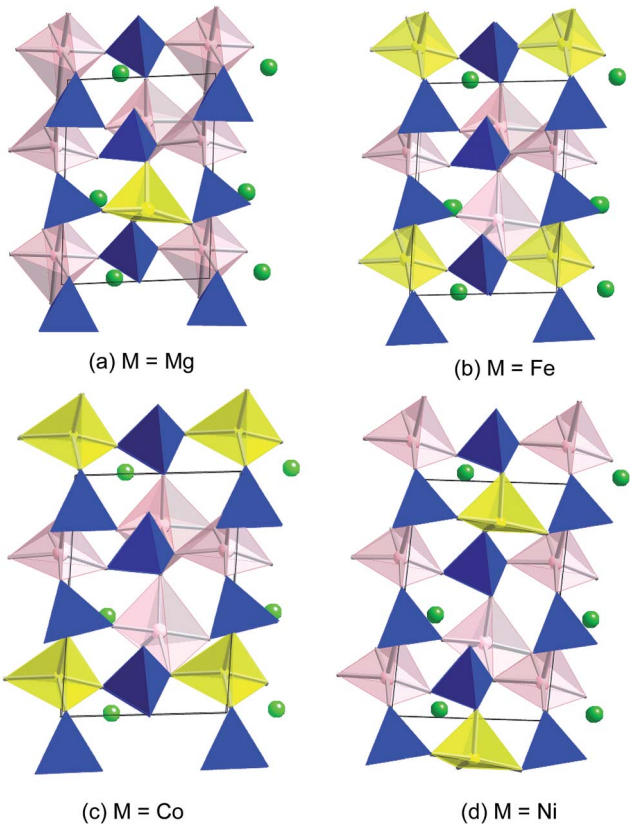

Fig. 5 Ground-state geometries of $Li_{0.5}Mn_{0.75}M_{0.25}SiO_4$ (a) M = Mg, (b) M = Fe, (c) M = Co and (d) M = Ni. Color code: Li, green; Mn, pink; M, yellow; and Si, blue.

The most stable configurations for Mg, Fe and Co substituents (Fig. 5a–c) possess Mn^{4+} in octahedral coordination, sharing edges with the adjacent Si and Mn polyhedra. Ni is the only investigated TM ion which does not produce octahedral Mn^{4+} in any configuration. Indeed, as seen in Fig. 4, configurations 1, 3 and 4 consist of tetrahedral Mn ions. The most stable configuration (Fig. 5d) is built up by Mn ions in five-fold coordination (see Table 2 in the ESI†), having edge sharing Mn–Mn contacts. Even if Mn^{4+} ions are more stable in octahedral coordination (Table 1), the effect of the Ni^{2+} substituent is to stabilize Mn^{4+} in five-fold coordination. This suggests that Ni^{2+} might be an efficient substituent to ameliorate the structural distortion. All the substituted $Li_{0.5}Mn_{0.75}M_{0.25}SiO_4$ compounds have greater volume than the Mn only parent compound, among them Ni produces the largest cell (76.1 $Å^3$

per f.u.). This is not surprising since $Li_{0.5}Mn_{0.75}Ni_{0.25}SiO_4$ comprises non-oxidized Ni^{+2} ions (see ESI†). The larger volume of the delithiated phase is beneficial since it implies a lower volume contraction respective to the initial phase.

Ni is a possible candidate to ameliorate the structural distortion suffered by Li_2MnSiO_4 due to the oxidation of Mn^{2+} to Mn^{4+} upon delithiation. Previous DFT work predicts that Li_2NiSiO_4 has very high de-intercalation voltages, 4.5 V for the Ni^{2+}/Ni^{3+} couple and 5.2 V for the Ni^{3+}/Ni^{4+} couple. We can thus expect that Ni substitution would increase the average de-insertion voltage of Li_2MnSiO_4. Even though achieving the full capacity of $Li_2Mn_{1-x}Ni_xSiO_4$ electrode materials would be impracticable, they might display better capacity retention upon cycling than Li_2MnSiO_4.

(C) Experimental investigation of $Li_2Mn_{1-x}Ni_xSiO_4$

Fig. 6 shows the XRD patterns collected from as-synthesized Li_2MnSiO_4, and the substituted $Li_2Mn_{1-x}Ni_xSiO_4$ samples with $x = 0.1$ and 0.2. A close view of the (011) peak at about 24.25 degrees of $x = 0$, 0.1, 0.2 showed Vegard's shift due to Ni substitution. The refined lattice parameters are given in Table 2; a decrease can be seen in all three lattice parameters (see also Fig. S3†). The parameter decreases are expected, as Ni^{2+} in a tetrahedral configuration has a smaller ionic radius than Mn^{2+} in a tetrahedral configuration. For the nominal composition of $Li_2Mn_{0.9}Ni_{0.1}SiO_4$ the ICP analysis yields Ni and Mn contents of 0.0944 ± 3.6%, and 0.9056 ± 3.6%, respectively. The Ni/Mn content in $Li_2Mn_{0.8}Ni_{0.2}SiO_4$ has also been confirmed by ICP analysis (Ni: 0.218 ± 1.7%, Mn: 0.782 ± 1.7%). Attempts to prepare $Li_2Mn_{1-x}Ni_xSiO_4$ samples with higher x contents were unsuccessful.

Fig. 7 shows the SEM of the $Li_2Mn_{1-x}Ni_xSiO_4$ samples with $x = 0$, 0.1 and 0.2. They all contain aggregates of small rounded particles. The average particle size is about 100 nm for $x = 0$ and 0.1. For $x = 0.2$, some larger plate-like particles are distinguished in the spherical aggregates. Regardless of the small particle size, the as-prepared samples displayed a poor electrochemical behaviour (see Fig. 4 in ESI†), making carbon coating a necessary treatment. Examining the XRD patterns of the carbon coated samples (shown in Fig. 5 of ESI†) the formation of a second phase is observed; due to the reducing conditions Ni has segregated from the samples, as evidenced by the peaks at about 45 and 52 degrees which are attributable to Ni metal (ICSD Collection Number #41508). We cannot ensure that the segregation of Ni from the sample is complete; hence some Ni may remain in the structure. In short, the real Ni content in $Li_2Mn_{1-x}Ni_xSiO_4$ carbon coated materials is unknown.

The electrochemical behaviour of the $Li_2Mn_{1-y}Ni_ySiO_4$ coated samples is shown in Fig. 8a–c. As evidenced in Fig. 2, regardless of the carbon coating, the prepared Li_2MnSiO_4 electrode suffers from an important polarization, hence showing a lower specific capacity than that found in ref. 24. Nevertheless, in all the $Li_2Mn_{1-x}Ni_xSiO_4$ materials, the voltage profile changes

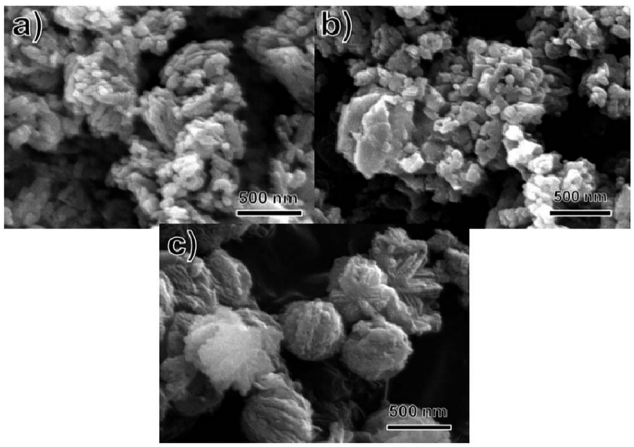

Fig. 7 SEM images of $Li_2Mn_{1-x}Ni_xSiO_4$ samples (a) $x = 0$, (b) $x = 0.1$ and (c) $x = 0.2$ prepared by the solvothermal method.

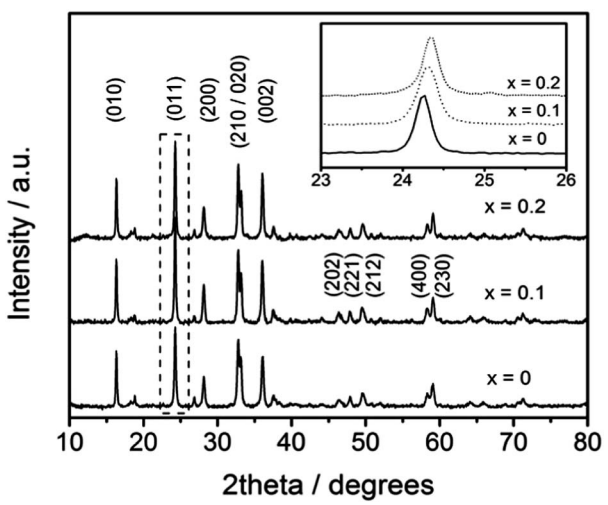

Fig. 6 Powder X-ray diffraction patterns of $Li_2Mn_{1-x}Ni_xSiO_4$ samples prepared by the solvothermal method. The inset shows the shift of the (0 1 1) reflection with Ni content.

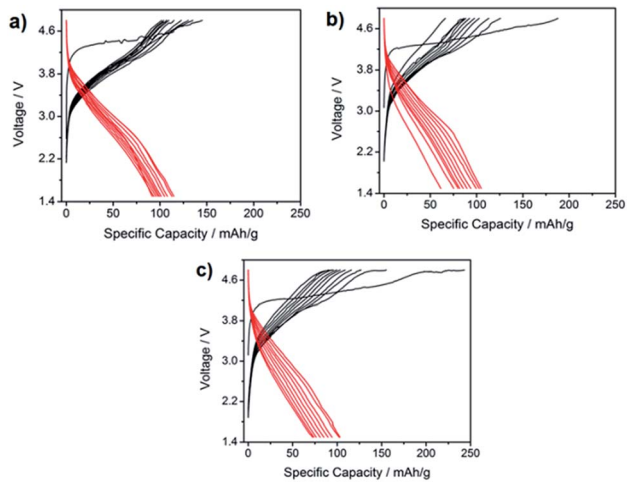

Fig. 8 Comparison of the electrochemical cycling profile of pristine Li_2MnSiO_4 (a) and the Ni substituted samples $Li_2Mn_{0.9}Ni_{0.1}SiO_4$ (b) and $Li_2Mn_{0.8}Ni_{0.2}SiO_4$ (c). A voltage window of 4.8–1.5 V was used at a C/20 rate.

from the first to the second charge which is indicative of major crystal structure modifications. The first charge capacities are 150 mA h g^{-1} for $x = 0$, 180 mA h g^{-1} for $x = 0.1$ and 250 mA h g^{-1} for $x = 0.2$. The increasing capacity with the nominal Ni content in the sample suggests that some of the Ni might remain in the silicate structure. However, as discussed below, we cannot exclude that part of the delivered capacity is due to electrolyte decomposition.

Fig. 9 shows the capacity retention with cycling of $Li_2Mn_{1-x}Ni_xSiO_4$ coated samples. The materials are able to show reversible capacities exceeding 100 mA h g^{-1} after the first discharge and stable charge and discharge capacities for the first 10 cycles. This reversible capacity corresponds to the cycling of 0.7 Li ions in Li_2MnSiO_4, consistently with the computational results evidencing that major structural rearrangement has already occurred at half delithiation. No improvement is observed for the Ni doped samples, which is likely due to its segregation from the crystal structure.

Ex situ XPS spectra were collected during the initial charge of a $Li//Li_2Mn_{0.8}Ni_{0.2}SiO_4$ cell at the pristine state, charged to 4.5 V and charged to 4.8 V (see Fig. 6 in the ESI†). Fig. 10 shows the collected spectra of Mn2p, Ni2p, C1s, and Si2p. The $Mn2p^{3/2}$ peak is made of two components corresponding to Mn^{2+} at 643.0 eV and Mn^{3+} at 646.5 eV. During charging, the intensity of the Mn^{2+} peak decreases while the intensity of the Mn^{3+} peak increases indicating oxidation of Mn on the surface of the material. However, the Ni 2p peak does not change during charging likely due to Ni precipitation as metallic nanoparticles. The C 1s spectra show signals typical of composite electrode materials including adventitious carbon at 284.6 eV, CH_2 bonds at 285.3 eV and CF_2 bonds at 290.7 eV due to the PVdF binder. There is a gradual increase in the intensity of the 287.2 eV peak which is attributed to C–O bonds corresponding to electrolyte (EC : DMC) decomposition at high voltages. The Si 2p spectra show an interesting reaction between Si and F after charging due to the formation of a peak at 106.4 eV while the Si–O bond at 102.9 eV remains the same. There could be etching of the SiO_4 framework by small amounts of HF in the electrolyte which forms Si–F bonds. XPS spectra of delithiated $Li_2Mn_{0.8}Ni_{0.2}SiO_4$ samples confirm the oxidation of Mn^{2+}, inactivity of Ni, and possible surface reactions between the SiO_4 framework and the electrolyte.

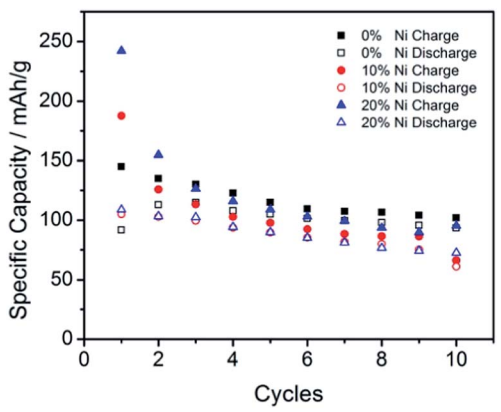

Fig. 9 Comparison of the capacity retention with cycling of pristine Li_2MnSiO_4 (black) and the Ni substituted samples $Li_2Mn_{0.9}Ni_{0.1}SiO_4$ (red) and $Li_2Mn_{0.8}Ni_{0.2}SiO_4$ (blue). A voltage window of 4.8–1.5 V was used at a C/20 rate.

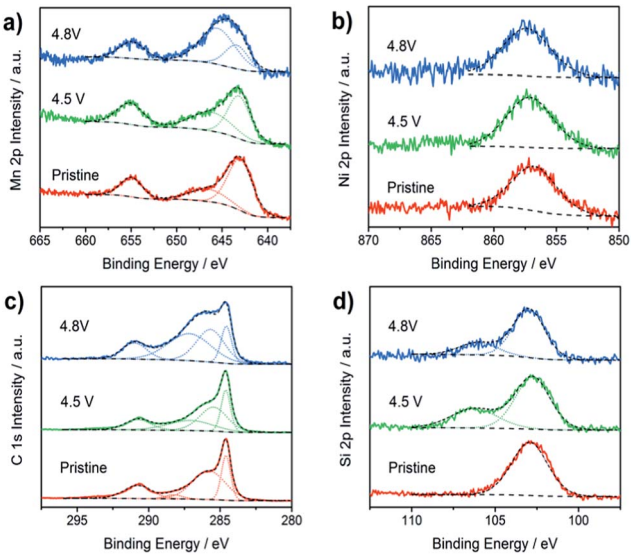

Fig. 10 *Ex situ* XPS collected during the first charge of a Li cell bearing $Li_2Mn_{0.8}Ni_{0.2}SiO_4$ as the positive electrode at pristine, charged to 4.5 V and charged to 4.8 V state of charge. (a) The Mn 2p spectra show a gradual tradeoff between Mn^{3+} at ~646.5 eV and Mn^{2+} at ~643.0 eV. (b) Ni 2p spectra do not change at all most likely due to its precipitation as metallic Ni nanoparticles. (c) C 1s spectra show typical peaks at 284.6 eV for adventitious carbon (C–C, C–H), PVdF binder peaks at 285.3 eV for (CH_2), and 290.7 eV for (CF_2). There is also a gradual increase in intensity of the C 1s peak at 287.2 eV which is due to (C–O) bonds corresponding to electrolyte decomposition. (d) The Si 2p spectra show a 102.9 eV peak for the Si–O bond in the silicate structure; but after charging, a new peak at 106.4 eV appears which corresponds to Si–F bonds.

Conclusions

First principles calculations have been utilized to rationalize the poor electrochemical performance of Li_2MnSiO_4. A large number of 142 $Li_{2y}MnSiO_4$ configurations have been examined. Computational results demonstrate that important crystal structure modifications in the Li_2MnSiO_4 electrode material have already occurred at half delithiation. The irreversible structural changes are linked to severe local distortions around the Mn^{2+} polyhedron upon delithiation. Since the lost of tetrahedral coordination of Mn^{2+} is rooted in the crystal field stabilization of Mn^{4+} and Mn^{3+} in higher coordination numbers, such structural distortions cannot be avoided. This explains the difficulties in (i) extracting more than one Li ion from Li_2MnSiO_4 and (ii) holding the capacity retention with cycling even for the first electron process. In this sense, Li_2MnSiO_4 is not competitive as the positive electrode material in Li cells. Yet we have investigated if crystal structure distortions during the charge of the cell could be minimized by partially substituting Mn ions with Mg, Fe, Co and Ni. We infer

that among these substituents, only Ni would barely help to ameliorate the structural distortion upon lithium de-insertion.

Ni substitution of Mn in $Li_2Mn_{1-x}Ni_xSiO_4$ was successfully achieved up to $x = 0.2$ by solvothermal synthesis. To make the materials electrochemically active, carbon coating was necessary. The reducing conditions of the carbon coating process (high temperature heating in Ar) caused the reduction of Ni^{2+} from the $Li_2Mn_{1-x}Ni_xSiO_4$ materials, and its precipitation as Ni nanoparticles. $Li_2Mn_{1-x}Ni_xSiO_4$ materials display a good capacity retention with cycling, but limited to only 100 mA h g^{-1} (0.7 Li ions in Li_2MSiO_4), as encountered in the parent Li_2MnSiO_4. The poor electrochemical behaviour of $Li_2Mn_{1-x}Ni_xSiO_4$ is attributed to the almost total segregation of Ni^{+2} from the silicate structure.

Based on the computational results we discarded Mg, Fe and Co as possible Mn substituents to enhance the electrode characteristics of Li_2MnSiO_4. On the contrary, DFT calculations suggest that Ni^{2+} could help to retain the crystal structure of charged $Li_{2y}MnSiO_4$ electrodes, improving the specific capacity delivered by the electrode and its retention with cycling. However, our experimental approach failed to retain Ni^{2+} in the initial $Li_2Mn_{1-x}Ni_xSiO_4$ crystal structure during the conformation of the electrode. Further work is needed to modify the carbon-coating conditions. In addition, future work combining experiments and calculations is desirable to screen for other chemical modifications likely to improve the electrochemical performance of Li_2MnSiO_4.

Acknowledgements

M. E. Arroyo acknowledges Ministerio de Ciencia e Innovación for grants MAT 2011-22753 and CSD2007-00045. M. E. Arroyo and A. Saracibar are grateful for computer time to the Spanish's national high performance computer service *via* the Barcelona Supercomputer and the I2 Basque Centres. Y. S. Meng, Z. Wang and K. Carroll acknowledge the UCSD faculty startup fund and Qualcomm gift fund. The authors are indebted to T. Muraliganth and A. Manthiram for kindly sharing their experimental data to confront with computations.

References

1 A. Nyten, A. Abouimrane, M. Armand, T. Gustafsson and J. O. Thomas, *Electrochem. Commun.*, 2005, **7**, 156.
2 R. Dominko, M. Bele, M. Gaberščček, A. Meden, M. Remškar and J. Jamnik, *Electrochem. Commun.*, 2006, **8**, 217.
3 C. Lyness, B. Delobel, A. R. Armstrong and P. Bruce, *Chem. Commun.*, 2007, **46**, 4890.
4 M. S. Islam, R. Dominko, C. Masquelier, C. Sirisopanaporn, A. R. Armstrong and P. Bruce, *J. Mater. Chem.*, 2011, **21**, 9811.
5 M. E. Arroyo-de Dompablo, M. Armand, J.-M. Tarascon and U. Amador, *Electrochem. Commun.*, 2006, **8**, 1292.
6 A. R. West and F. P. Glasser, *J. Solid State Chem.*, 1972, **4**, 20.
7 M. E. Arroyo-de Dompablo, R. Dominko, J. M. Gallardo-Amores, L. Dupont, G. Mali, H. Ehrenberg, J. Jamnik and E. Moran, *Chem. Mater.*, 2008, **20**, 5574.
8 C. Sirisopanaporn, C. Masquelier, P. Bruce, A. R. Armstrong and R. Dominko, *J. Am. Chem. Soc.*, 2011, **133**, 1263.
9 A. Saracibar, A. Van de Ven and M. E. Arroyo y de Dompablo, *Chem. Mater.*, 2012, **24**, 495.
10 R. J. Gummow and Y. He, *J. Power Sources*, 2014, **253**, 315.
11 R. Dominko, L. Arcon, A. Kodre, D. Hanzel and M. Gaberscek, *J. Power Sources*, 2009, **189**, 51.
12 D. M. Kempaiah, D. Rangappa and I. Honma, *Chem. Commun.*, 2012, **48**, 2698.
13 A. Kokalj, R. Dominko, G. Mali, A. Meden, M. Gaberscek and J. Jamnik, *Chem. Mater.*, 2007, **19**(15), 3633.
14 M. Kuezma, S. Devaraj and P. Balaya, *J. Mater. Chem.*, 2012, **22**, 21279.
15 T. Muraliganth, K. R. Stroukoff and A. Manthiram, *Chem. Mater.*, 2010, **22**, 5754.
16 A. I. Liechtenstein, V. I. Anisimov and J. Zaanen, *Phys. Rev. B: Condens. Matter Mater. Phys.*, 1995, **52**, R5467.
17 G. Kresse and J. Furthmuller, *Phys. Rev. B: Condens. Matter Mater. Phys.*, 1996, **54**, 11169.
18 G. Kresse and J. Furthmuller, *Comput. Mater. Sci.*, 1996, **15**, 6.
19 P. E. Bloch, *Phys. Rev. B: Condens. Matter Mater. Phys.*, 1994, **50**, 17953.
20 S. L. Dudarev, G. A. Botton, S. Y. Savrasov, Z. Szotek, W. M. Temmerman and A. P. Sutton, *Phys. Status Solidi A*, 1998, **166**, 429.
21 A. Van der Ven, J. C. Thomas, Q. Xu, B. Swoboda and D. Morgan, *Phys. Rev. B: Condens. Matter Mater. Phys.*, 2008, **78**, 104306.
22 A. Van der Ven, J. C. Thomas, Q. Xu, B. Swoboda and J. Bhattacharga, *Mathematical and Computers in Simulation*, 2010, **80**, 1393.
23 V. Aravindan, K. Karthikeyan, J. W. Lee, S. Madhavi and Y. S. Lee, *J. Phys. D: Appl. Phys.*, 2011, **44**, 152001.
24 T. Muraliganth, K. R. Stroukoff and A. Manthiram, *Chem. Mater.*, 2010, **22**, 5754.
25 P. Larsson, A. Raajev, A. Liivat and J. O. Thomas, *Comput. Mater. Sci.*, 2010, **47**, 678.
26 G. Ceder and A. Van der Ven, *Electrochim. Acta*, 1999, **45**, 131.
27 A. Van der Ven and G. Ceder, in *Lithium Batteries: Science and Technology*, ed. G. Nazri and G. Pistoia, Kluwer Academic Publishers, 2004.
28 H. Lee, S. Park, J. Moon, H. Lee, K. Cho, M. Cho and S. Kim, *Chem. Mater.*, 2014, **26**, 3896.